# Determining Chondritic Impactor Size from the Marine Osmium Isotope Record

François S. Paquay, *et al.*

*Science* **320**, 214 (2008);
DOI: 10.1126/science.1152860



*Science* (print ISSN 0036-8075; online ISSN 1095-9203) is published weekly, except the last week in December, by the American Association for the Advancement of Science, 1200 New York Avenue NW, Washington, DC 20005. 

a GSL curve, giving the GSL variation that would have been free from the impact of artificial reservoirs, it becomes evident that, in contrast to the observations, the post-1930 GSL rose essentially at a constant rate all the way to the recent years (barring any interspersed interannual fluctuations such as El Niño–Southern Oscillation events or volcanic activities) at a rate of +2.46 mm/year, versus an average of +1.7 to 1.8 mm/year during the 20th century with recent acceleration. Whether this means that the global changes causing the GSL rise have been in operation in a rather steady fashion, or instead fortuitously compensated one another over at least the past 80 years, remains to be examined.

Our findings differ from the conventional wisdom, which holds an apparent variable GSL rise according to the face values of observation as stated above. This, of course, by no means precludes the most recent or possible future acceleration of GSL rise (*23*) due to natural causes, compounded by the further slowdown of reservoir-building in the near future (*26*).

### References and Notes


1. N. L. Bindoff *et al.*, in *Climate Change 2007: The Physical Science Basis. Contribution of Working Group I to the Fourth Assessment Report of the Intergovernmental Panel on Climate Change*, S. Solomon *et al.*, Eds. (Cambridge Univ. Press, New York, 2007), chap. 5.
2. W. S. Newman, R. W. Fairbridge, *Nature* **320**, 319 (1986).
3. B. F. Chao, *Eos* **72**, 492 (1991).
4. B. F. Chao, *Geophys. Res. Lett.* **22**, 3533 (1995).
5. V. Gornitz, C. Rosenzweig, D. Hillel, *Global Planet. Change* **14**, 147 (1997).
6. V. Gornitz, in *Sea Level Rise*, B. Douglas, M. Kearney, S. Leatherman, Eds. (Academic Press, London, 2001).
7. D. L. Sahagian, *Global Planet. Change* **25**, 39 (2000).
8. D. L. Sahagian, F. W. Schwartz, D. K. Jacobs, *Nature* **367**, 54 (1994).
9. *World Register of Dams* (International Commission on Large Dams, Paris, 2007) (www.icold-cigb.net).
10. F. van der Leeden, *Water Resources of the World* (Water Information Center Inc., New York, 1975).
11. *World Water Balance and Water Resources of the Earth* (UNESCO, Paris, 1978).
12. U.S. Department of the Interior, *Major Dams, Reservoirs, and Hydroelectric Plants* (Bureau of Reclamation, Denver, 1983).
13. *International Water Power & Dam Construction Handbook*, R. M. Taylor, Ed. (Reed Business, Surrey, UK, 1993).
14. World Commission on Dams, *Dams and Development* (Earthscan, London, 2000).
15. UNESCO, *World Water Resources at the Beginning of the 21st Century* (Cambridge Univ. Press, New York, 2003).
16. W. W. Storage, *in Man-Made Reservoirs* (Foundation for Water Research, Marlow, UK, 2005).
17. See supporting material on *Science* Online.
18. Different (least-squares) fit ranges and bin widths were tried; the results vary little.
19. The rapid convergence of the extrapolated integration, consistent with (*20*), down to small reservoir size is assured as follows. For a self-similar fractal "map" distribution of self-similar reservoirs with respect to the linear dimension $L$, the reservoir number decreases as $L^{-2}$ while the corresponding volume increases as $L^3$. Hence, the water impoundment for a given size increases as $L$, dominated by large reservoirs. The actual reservoir number increases with smaller size even more slowly than the above, only at $L^{-1.56}$ ($-1.56 = -0.52 \times 3$). The situation is analogous to the (Richter-Gutenberg) frequency-moment relationship for seismicity, where the "β value" (or the negative of the power-law slope) is ⅔, hence the total seismic energy release is dominated by large earthquakes even though the smaller earthquakes are much more numerous.
20. M. I. L'vovich, G. F. White, in *The Earth as Transformed by Human Action*, B. L. Turner II *et al.*, Eds. (Cambridge Univ. Press, Cambridge, 1990).
21. P. C. D. Milly *et al.*, position paper, World Climate Research Programme Workshop on Understanding Sea-Level Rise and Variability (UNESCO, Paris, 2006).
22. By comparison, in terms of GSL the total atmospheric water content is equivalent to ~35 mm and the total biological water is equivalent to ~3 mm.
23. B. D. Beckley, F. G. Lemoine, S. B. Luthcke, R. D. Ray, N. P. Zelensky, *Geophys. Res. Lett.* **34**, L14608 (2007).
24. Among other anthropogenic (positive) contributions to GSL, groundwater mining (mainly for irrigation) is potentially important (*1*, *5*–*7*), which partially offsets the impact of the reservoir impoundment. Its amount is considerably smaller (*6*), albeit far less certain, than the reservoirs', and presumably grew over the decades with a different time signature. A separate assessment is needed.
25. J. A. Church, N. J. White, *Geophys. Res. Lett.* **33**, L01602 (2006).
26. The slowdown is already evident in Fig. 1, which includes the projection into the next few years according to our tally (for example, $d = -30.6$ mm by 2010), although late reporting of reservoir-building may have also contributed to the apparent slowdown.


27. We thank J. Church, R. Ray, D. Sahagian, A. Cazenave, C. K. Shum, L. Y. Tsai, S. T. Li, and L. Lin for discussions and assistance. Supported by the Taiwan Semiconductor Manufacturing Company Ltd. Chair professorship and by National Science Council of Taiwan grant NSC96-2111-M-008-016-MY2.


### Supporting Online Material

www.sciencemag.org/cgi/content/full/1154580/DC1
Materials and Methods
Table S1


26 December 2007; accepted 5 March 2008
Published online 13 March 2008;
10.1126/science.1154580
Include this information when citing this paper.


# Determining Chondritic Impactor Size from the Marine Osmium Isotope Record


**François S. Paquay,[1]* Gregory E. Ravizza,[1] Tarun K. Dalai,[1]† Bernhard Peucker-Ehrenbrink[2]**



**Decreases in the seawater $^{187}Os/^{188}Os$ ratio caused by the impact of a chondritic meteorite are indicative of projectile size, if the soluble fraction of osmium carried by the impacting body is known. Resulting diameter estimates of the Late Eocene and Cretaceous/Paleogene projectiles are within 50% of independent estimates derived from iridium data, assuming total vaporization and dissolution of osmium in seawater. The variations of $^{187}Os/^{188}Os$ and Os/Ir across the Late Eocene impact-event horizon support the main assumptions required to estimate the projectile diameter. Chondritic impacts as small as 2 kilometers in diameter should produce observable excursions in the marine osmium isotope record, suggesting that previously unrecognized impact events can be identified by this method.**


Terrestrial and lunar impact craters, as well as impact debris in the sediment record, reveal that Earth has been struck by asteroids many times throughout its history. However, it is difficult to estimate the size of the impacting bodies, and it is likely that many impacts remain unrecognized because of the continuous reshaping of Earth's surface. Rough estimates of projectile size result from inventories of excess Ir (*1*), called Ir fluences (nanograms per square centimeter), and from models of impact-crater formation (*2*). The former approach involves averaging many individual fluence estimates to obtain a meaningful global signal (*3*–*5*), whereas the latter approach requires that an impact crater be preserved.

Since the first application of the Os isotopic system to the study of impact events (*6*), this system has been extensively applied to estimating the contribution of the projectile to impact breccias and impact melts (*7*). These studies report high Os concentrations and low $^{187}Os/^{188}Os$ ratios of the projectile compared with the target rock, demonstrating that Os isotopes are very sensitive tracers of the presence of residual projectile material. Most previous Os isotope studies of impact events have focused narrowly on the impact horizon (*6*–*11*). However, Os isotope studies of the marine sediment record that span longer time intervals show that the dissolution of impact-derived Os in seawater lowers the $^{187}Os/^{188}Os$ values of the global ocean (*12*, *13*).

We show here that impact-induced excursions in the marine Os isotope record can be used to estimate chondritic impactor size (*14*). These excursions can be understood as the result of mixing ambient seawater Os (characterized by relatively high $^{187}Os/^{188}Os$) with meteoritic Os [with low $^{187}Os/^{188}Os$ (*15*)] that is vaporized on impact and subsequently dissolved in seawater. This interpretive framework allows for the estimation of


[1]Department of Geology and Geophysics, University of Hawaii, Honolulu, HI 96822–2225, USA. [2]Department of Marine Chemistry and Geochemistry, Woods Hole Oceanographic Institution, Woods Hole, MA 02543, USA.

*To whom correspondence should be addressed. E-mail: paquay@hawaii.edu

†Present address: Department of Geology and Geophysics, Indian Institute of Technology, Kharagpur 721302, India.

projectile size by isotope dilution, provided that the fraction of impact-derived Os that dissolves in seawater is known. The Os isotope composition of seawater is nearly homogeneous, so data from only a single section that accurately records seawater $^{187}Os/^{188}Os$ can be used to make meaningful estimates of projectile size. No analogous variations in Ir isotope composition occur in nature, making the Os isotope system unique among the highly siderophile elements.

As an example, we applied this approach to the known Late Eocene impacts (LEIs) (*16*) and the Cretaceous-Tertiary (K-T) impact (*1*) events. The three key parameters that we used to estimate the fractional increase in the seawater Os reservoir that results from an impact are the $^{187}Os/^{188}Os$ of seawater immediately before and after the impact event (*17*) and the $^{187}Os/^{188}Os$ of the impacting body, which varies over a narrow range (0.123 to 0.129) (*15*). During the LEIs, seawater $^{187}Os/^{188}Os$ shifted from 0.5 to 0.28 (Fig. 1 and table S1), corresponding to a roughly 2.5-fold increase in the size of the seawater Os reservoir because of the impact-derived Os (*18*). Agreement between data from the equatorial Pacific [Ocean Drilling Program (ODP) 1219] and the Southern Ocean (ODP 1090) indicates that these data reflect the response of seawater $^{187}Os/^{188}Os$ to the impacts, rather than mixing of particulate Os from different sources. We suspect that the time required for the impact-induced Os isotope excursion to mix throughout the global ocean is brief, on the order of several thousand years. However, the decline in the sediment $^{187}Os/^{188}Os$ from preimpact levels to minimum values is ~30 to 40 thousand years (ky). The length scale of this decline is 110 to 130 cm, consistent with limited redistribution by diagenesis and/or bioturbation. The Os isotope shift derived from a low-resolution record of the K-T event ranges from 0.4 to 0.157 (Fig. 2), indicating a nearly 10-fold increase in seawater Os inventory.

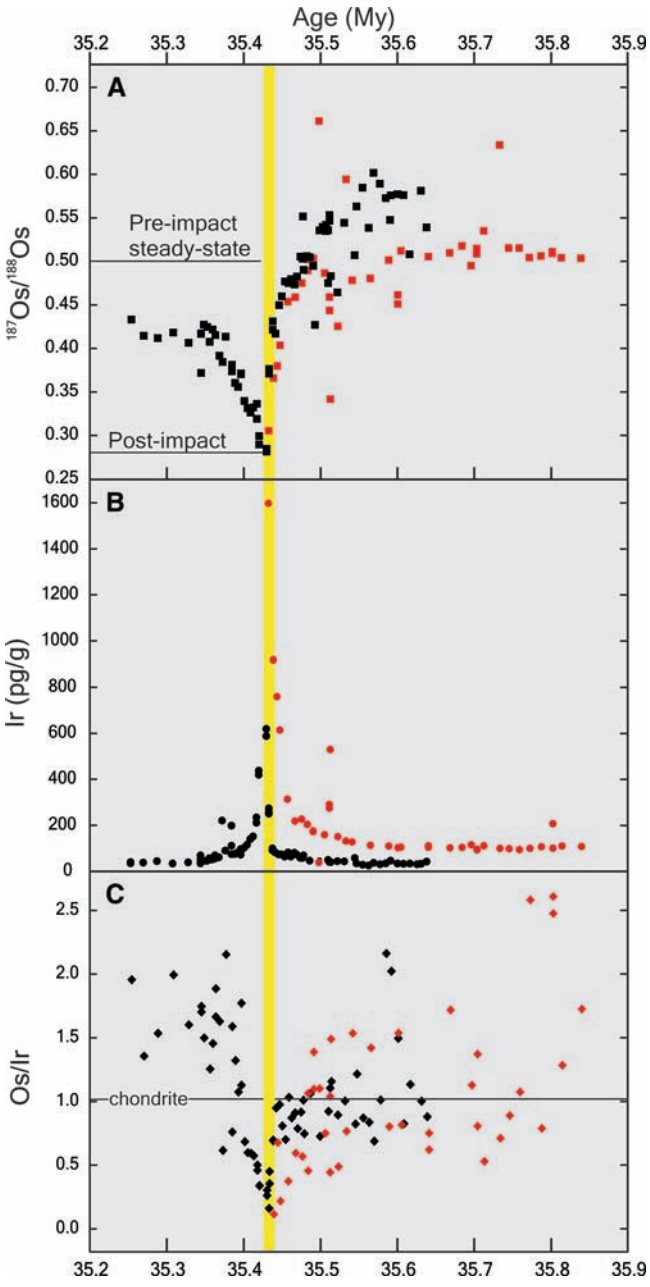


**Fig. 1.** Profiles of $^{187}Os/^{188}Os$ ratios, Ir concentrations, and Os/Ir ratios from ODP 1219 (7°48.01′N, 142°00.94′W) and ODP 1090 (42°54.8′S, 8°54.0′E). Age control is based on magnetic stratigraphy (*44*, *45*). Most samples are from within magnetochron C16n.1n. Sediments from Site 1219 deposited immediately after the LEIs were unavailable for analysis because of a gap between cores and limited drilling disturbance. Black symbols represent ODP Site 1090; red symbols represent ODP 1219. My, million years. (**A**) Minimum values in $^{187}Os/^{188}Os$ coincide with the Ir maximum, defining an asymmetric excursion with an abrupt onset and gradual recovery. The yellow line indicates the impact horizon. (**B**) Elevated Ir concentrations mark the impact horizon. In ODP Site 1090, clino-pyroxene spherules and microtektites were recognized and coincide with maximum Ir concentrations (*20*). (**C**) At both sites, local maxima in Os concentration are much less pronounced than those in Ir. Os/Ir ratios therefore display a clear minimum at the impact horizon.

A quantitative comparison of the Os isotope method to independent Ir fluence estimates can be made by assuming that the Os concentration of Late Eocene and Late Cretaceous seawater is the same as that of the modern ocean (*19*). This fixes the preimpact size of the seawater Os reservoir at $1.4 \times 10^{19}$ ng Os (*18*) and allows the mass of impact-derived Os dissolved in the ocean after the LEI ($2 \times 10^{19}$ ng Os) and K-T events ($8 \times 10^{19}$ ng Os) to be calculated. These Os inventories are between 30 and 40% of the Ir inventories for the LEI ($4.6 \times 10^{19}$ ng Ir) and K-T events ($28 \times 10^{19}$ ng Ir), calculated as the product of the average global Ir fluence [LEI = 9 ng/cm$^2$ (*20*) and K-T = 55 ± 3 ng/cm$^2$ (*3*)] and the surface area of Earth. Os and Ir inventories can be compared directly because the Os/Ir ratio in chondrites (*15*, *21*) is close to 1. We suspect that the deficit of Os relative to Ir probably results from nonquantitative dissolution of Os in seawater, but the uncertainties in the estimated Os and Ir fluences are too large to argue this point strongly (*22*). Nevertheless, observations that some terrestrial K-T sections are enriched in Os (*7*) are consistent with the idea that Os dissolution is incomplete and Os isotope-based estimates of projectile size that assume quantitative vaporization are biased to low values.

The Os and Ir inventories estimated above can be recast as projectile-size estimates (*23*). The Popigai impactor associated with the LEIs is thought to be an L-type ordinary chondrite (*24*). Using appropriate average bulk density (*25*) and Os and Ir concentrations (*21*) yields an Os-based diameter estimate of 2.8 to 3.0 km for the Popigai impactor (*26*), compared with an Ir-based diameter estimate of 4 km (*27*). For the K-T event, a carbonaceous chondrite (*11*, *28*) is the likely culprit, and analogous calculations yield diameter

estimates of 4.1 to 4.4 and 6 km, based on Os isotopes (*23*) and Ir fluence (*27*), respectively. The smaller size of the Os-based estimates (as compared with Ir is a direct consequence of the relative magnitude of the Os and Ir inventories given above. The most recent simulations of impact-crater formation yielded projectile-size estimates of 15 to 19 km for the K-T Chixulub crater (*2*), 8 km for the Late Eocene Popigai crater (*2*), and 3 km for the Late Eocene Chesapeake Bay crater (*29*, *30*). If these larger projectile-size estimates are correct, this implies that only 2 to 7% of the Os carried by the K-T and LEI projectiles dissolved in seawater. The box-model results below suggest that substantially more than a few percent of the total amount of Os carried by the projectile becomes dissolved in seawater. An important implication of this interpretation is that impact simulations overestimate the projectile diameter. The relatively good agreement between diameter estimates based on Os isotopes and Ir fluence is consistent with this inference. Whereas the choice of projectile velocity and angle of incidence might contribute to the difference in estimated projectile sizes, we do not believe that this is the sole source of the discrepancy. A projectile with substantially lower siderophile-element concentration than any known chondrite—perhaps a comet (*20*)—could account for this difference. However, no independent data are available to support this claim for either the K-T impact events or the LEIs.

Our interpretation requires that dissolved Os and Ir concentrations in the open ocean greatly exceed steady-state values immediately after an impact event. A box model that simulates the postimpact removal of excess dissolved Os and Ir from seawater by first-order kinetics captures the major features preserved in Late Eocene sediments from ODP Site 1090 (Fig. 3). We used initial conditions that correspond to dissolved Os concentrations that are elevated 2.5 times above steady-state levels with an initial postimpact $^{187}Os/^{188}Os$ of 0.28 (Fig. 1). These conditions were chosen to match the estimates of seawater and projectile-derived Os inventories made above. To simulate Ir removal from seawater, we assumed equal masses of impact-derived Os and Ir ($2 \times 10^{19}$ ng). This assumption, together with the very low Ir concentration of modern seawater (*31*) as compared with that of Os (*19*), resulted in model initial conditions where dissolved Ir was elevated 50 times above steady-state levels. The postimpact steady state $^{187}Os/^{188}Os$ was set at 0.42 to match the postimpact sediment data (Fig. 3A). The Os/Ir ratio of modern seawater is ~100 (*20*), whereas the Os/Ir ratio of modern pelagic carbonates falls between 2 and 3 (*21*). This difference indicates more rapid scavenging of Ir relative to Os in the open ocean. Therefore, to compare measured sediment Os/Ir ratios to model seawater ratios, we used $(Os/Ir)_{sediment} = 0.02(Os/Ir)_{seawater}$ (see note S1 in the supporting online material for detailed information about the model). The change in the sediment $^{187}Os/^{188}Os$ and Os/Ir with time was visually fit by adjusting the marine residence times of Os and Ir to match the sediment data (Fig. 3).

The comparison of model calculations with measured data yields estimated Late Eocene marine residence times of 25,000 years for Os and 5000 years for Ir. These values are similar to the modern marine residence-time estimates for Os and Ir—40,000 and 2000 years, respectively (*31*, *32*). The Os/Ir ratio calculated for Eocene

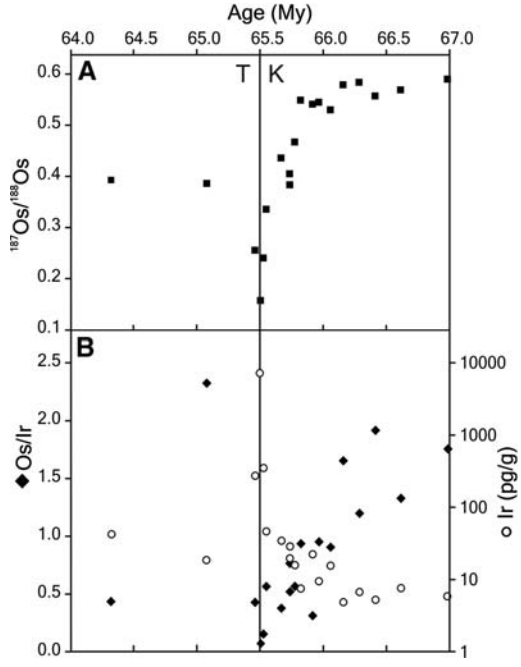


**Fig. 2.** (**A**) Low-resolution record of sediment $^{187}Os/^{188}Os$ across the K-T boundary in Deep Sea Drilling Project 577 (*13*). (**B**) Associated record of Ir and Os concentration variations from the same site. There is a distinct minimum in Os/Ir at the K-T boundary, similar to the pattern observed in the LEI event record (Fig. 1).

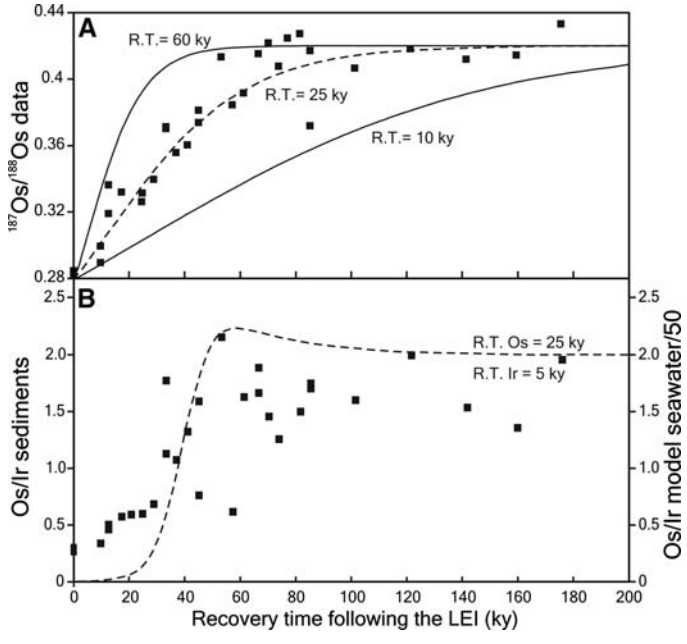


**Fig. 3.** Comparison of results from a one–box model simulation of recovery of seawater Os and Ir chemistry after the LEI impact event to data from ODP 1090 (Fig. 1). Initial conditions were chosen to mimic mixing the Os and Ir ($2 \times 10^{19}$ ng) with a seawater Os and Ir reservoir equivalent to that of the modern ocean. (**A**) We used a range of residence times (R.T.) for Os to fit the $^{187}Os/^{188}Os$ recovery with a visual best-fit at 25 ky (dashed line). The lower bound was set with an R.T. of 60 ky and the upper bound at 10 ky. (**B**) Os and Ir residence times were set at 25 and 5 ky, respectively [fractional increase in seawater reservoir (*18*) Os = 2.5 and Ir = 147]. The model Os/Ir curve (dashed line) was multiplied by 0.02 to allow a direct comparison of the range in Os/Ir measured in sediments to that of seawater.

seawater immediately after the impact (1.6) is initially close to the chondritic ratio of 1 and gradually recovers to higher values (Fig. 3B). The same trend is apparent in the ODP 1090 record, but the absolute Os/Ir ratios are shifted to distinctly subchondritic ratios as a result of preferential Ir scavenging as described above. The same pattern is also apparent in our low-resolution Os/Ir record spanning the K-T impact (Fig. 2). This simple model based on the behavior of Os and Ir in modern seawater yields reasonable residence-time estimates and can account for the observed sedimentary Os/Ir ratios. Thus, the major features of the ODP 1090 record can be understood as a result of the scavenging of dissolved elements from seawater without contributions from a large inventory of particulate Os or Ir from refractory phases that may have condensed in the atmosphere (*33*) and subsequently settled through the water column. Together with reported Os burial fluxes in pelagic sediments, Os residence-time estimates obtained from the model provide evidence that our assumption that the Os concentration of Late Eocene seawater is similar to that of the modern ocean is reasonable (*34*–*38*).

Paired Os/Ir and Os isotope records can also serve as an effective tool for distinguishing impact events, which vaporize Os and Ir and modify global seawater chemistry, from local enrichment of particulate extraterrestrial material. The latter could result from either a variable sediment-accumulation rate or fluctuation in the background flux of particulate extraterrestrial matter. Elevated Ir concentrations and lower $^{187}Os/^{188}Os$ could result from either an impact or particulate extraterrestrial matter. However, particle enrichment would not shift sediment Os/Ir to the distinctly subchondritic values observed in both Late Eocene records, because small unvaporized particles with chondritic Os/Ir ratios would accumulate intact. For example, some particulate extraterrestrial enrichment seems to characterize the Late Eocene sections of the ODP 1090 record before the impact events (Fig. 1). This may be causally linked to the episodes of increased flux of interplanetary dust particles inferred from $^{3}He$ data (*39*).

There are two distinctly different sources of uncertainty associated with the projectile-size estimates made here. The first is associated with the Os isotope-dilution calculation and the related assumptions about the dissolution of Os in seawater. The effects of these parameters on the projectile-diameter estimates are illustrated by sigmoidal curves (Fig. 4) showing that as the $^{187}Os/^{188}Os$ of postimpact seawater approaches that of the projectile (~0.13), error amplification becomes extremely large. This is important for K-T projectile-size estimates because small variations in boundary horizon $^{187}Os/^{188}Os$ can give rise to large changes in the projectile-size estimate (*40*). At the opposite end of the size spectrum, there is also substantial error amplification, corresponding to decreases in the seawater $^{187}Os/^{188}Os$ that are difficult to resolve from other sources of natural variability. The offset between the LEI and K-T fields in Fig. 4 illustrates the second source of uncertainty, which results from the need to constrain projectile Os concentration and bulk density by choosing a particular type of projectile. This offset provides a reasonable representation of the range of uncertainty introduced when the type of chondrite is unknown, because the Os concentration difference between the K-T and LEI projectile type spans nearly the maximum range in average Os concentrations among the major chondrite classes (*21*). Estimates of projectile size based on Ir fluence require equivalent assumptions about projectile type. An iron meteorite impact would produce an Os isotope excursion larger than that produced by a chondritic projectile of the same size (Fig. 4) because of higher densities (*25*) and larger Os concentrations (*41*). However, Cr isotopes (*11*) and $^{186}Os/^{188}Os$ (*9*) differentiate chondrites from irons and could be used to eliminate this potential source of uncertainty in projectile-size estimates.

The marine Os isotope record should also be sensitive to impact events smaller than the LEIs. For 30% dissolution of impact-derived Os in seawater, a 2-km chondritic body would produce a decrease of ~0.05 in seawater $^{187}Os/^{188}Os$ (Fig. 4). If only 5% of the total Os supplied by the projectile dissolves in seawater, as implied by impact-crater simulations (*2*, *41*), then a 4-km body would be reuired to produce the same magnitude of excursion (~0.05). The model results presented above suggest that it is probable that the fraction of the impact-derived Os dissolved in seawater is much larger than 5%, because the major features of the bulk sediment $^{187}Os/^{188}Os$ and Os/Ir records can be reproduced with a model in which the entire sedimentary Os and Ir inventories are scavenged from seawater. Based on observations of near-Earth asteroids, the estimated recurrence interval for bodies 4 km and larger is ~12 million years; for bodies 2 km and larger, it is ~2.5 million years (*42*). If correct, these recurrence intervals suggest that there should be between 5 and 27 impact-related excursions in the Cenozoic marine Os isotope record. Whereas we are confident that sediments recovered from the modern sea floor (like those studied here) will preserve the record of such events, we are not certain that older marine sequences now preserved on land will have the same fidelity.

Testing the lower limit of projectile detection warrants further investigation. The efficiency of Os and Ir vaporization may decrease with decreasing projectile size and may vary with target material. In addition, small regional heterogeneities in seawater $^{187}Os/^{188}Os$ [like those implied by the small offset between the ODP 1090 and 1219 records before LEIs (Fig. 1)] make it difficult to precisely estimate the $^{187}Os/^{188}Os$ of preimpact seawater. Both factors could make detection and size estimation of smaller impacts more difficult than is implied by Os isotope results from the larger K-T and LEI events. Other known Cenozoic impact craters provide an opportunity to investigate these issues. For example, the Ir-rich Eltanin asteroid [estimated at 1 to 4 km in size (*43*)] that hit the Pacific Ocean west of the southern end of South America in the Bellinghausen Sea is of particular interest because, in contrast to the LEI and K-T events, it is a deep-ocean impact.

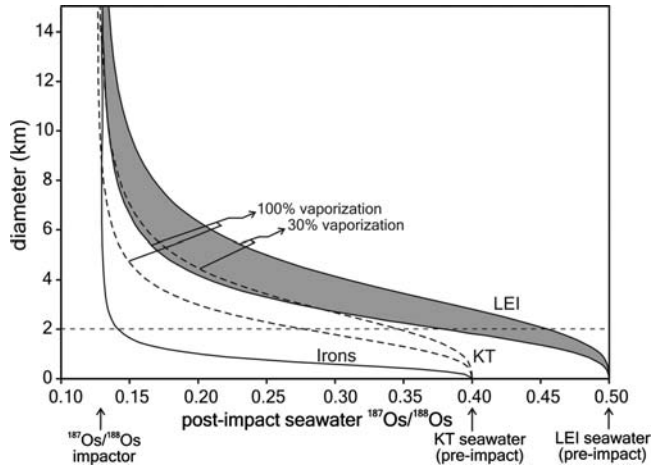


**Fig. 4.** Variation of estimated projectile diameter as a function of postimpact seawater $^{187}Os/^{188}Os$, projectile type, and fraction of Os vaporized. Projectile-diameter estimates are sensitive to the $^{187}Os/^{188}Os$ ratio of seawater before the impact and projectile Os concentration, requiring that the K-T boundary (white field bounded by dashed lines) and the LEI (gray field) be represented by different curves. The curve labeled "Irons," calculated with an average Os concentration of 30,000 ng/g (*40*) and a density of 8 g/cm$^3$ (*25*), predicts the strong influence of a relatively small iron meteorite on the $^{187}Os/^{188}Os$ of seawater. Projectiles as small as 2 km are expected to produce a detectable shift in $^{187}Os/^{188}Os$ (~0.05), assuming that 100% dissolution of impact-derived Os is soluble in seawater.

### References and Notes

1. L. W. Alvarez, W. Alvarez, F. Asaro, H. V. Michel, *Science* **208**, 1095 (1980).
2. B. A. Ivanov, *Sol. Syst. Res.* **39**, 381 (2005).
3. S. Donaldson, A. R. Hildebrand, *Meteorit. Planet. Sci.* **36** (suppl.), A50 (2001).
4. P. Claeys, W. Kiessling, W. Alvarez, *Geol. Soc. Am. Spec. Pap. 356* (2002), pp. 55–68.
5. A synthesis of existing Ir fluence data reveals a nearly 100-fold range in Ir fluence among the 55 sections studied to date (*3*). A review of data from the K-T

boundary shows maximum Ir concentrations ranging from 0.1 to 87 ng/g in 85 sections from deep marine to continental depositional environments (*4*).
6. J. M. Luck, K. K. Turekian, *Science* **222**, 613 (1983).
7. C. Koeberl, S. B. Shirey, *Palaeogeogr. Palaeoclimatol. Palaeoecol.* **132**, 25 (1997).
8. T. Meisel, U. Krähenbähl, M. A. Nazarov, *Geology* **23**, 313 (1995).
9. R. Frei, K. M. Frei, *Earth Planet. Sci. Lett.* **203**, 691 (2002).
10. D. G. Pearson *et al.*, *Geol. Soc. Am.* **31**, 123 (1999).
11. G. Quitté *et al.*, *Meteorit. Planet. Sci.* **42**, 1567 (2007).
12. B. Peucker-Ehrenbrink, G. E. Ravizza, A. W. Hofmann, *Earth Planet. Sci. Lett.* **130**, 155 (1995).
13. G. Ravizza, B. Peucker-Ehrenbrink, *Science* **302**, 1392 (2003).
14. The marine Os isotope record, like the Ir fluence approach, is not well suited to detecting the impact of differentiated projectiles, such as achondrites with siderophile-element concentrations that are two to three orders of magnitude lower than chondrites (*7*).
15. M. F. Horan, R. J. Walker, J. W. Morgan, J. N. Grossman, A. E. Rubin, *Chem. Geol.* **196**, 5 (2003).
16. J. Whitehead, D. A. Papanastassiou, J. G. Spray, R. A. F. Grieve, G. J. Wasserburg, *Earth Planet. Sci. Lett.* **181**, 473 (2000).
17. Methods and data table are available as supporting material on *Science* Online.
18. The increase in the seawater Os reservoir after an impact event is determined by knowing (i) the Os concentration in modern seawater (~10 pg/kg) (*19*) and (ii) the estimated mass of the seawater (~$1.4 \times 10^{21}$ kg). The product of these gives the mass of Os in the ocean before an impact [mass $Os_{sw}$ (ng)]. The mass of Os derived from the impactor [mass $Os_{impactor}$ (ng)] is $(f/1 - f) \times$ mass $Os_{sw}$; where $f = (^{187}Os/^{188}Os_{postimpact} - {}^{187}Os/^{188}Os_{preimpact})/(^{187}Os/^{188}Os_{impactor} - {}^{187}Os/^{188}Os_{preimpact})$. The fractional increase in the seawater Os reservoir is (mass $Os_{sw}$ + mass $Os_{impactor}$)/(mass $Os_{sw}$).
19. S. Levasseur, J.-L. Birck, C. J. Allègre, *Science* **282**, 272 (1998).
20. F. T. Kyte, S. Liu, *Lunar Planet. Sci.* **XXXIII**, 1981 (abstr.) (2002).
21. J. T. Wasson, G. W. Kallemeyn, *Philos. Trans. R. Soc. London Ser. A* **325**, 535 (1988).
22. A doubling of seawater Os concentration to 20 pg/kg would erase the Os deficit.
23. The diameter $D$ is estimated assuming a spherical projectile $D$ (km) = $\{2 \times [\text{mass } Os_{impactor} \times 3/[Os]_{impactor}$ (ng/g) $\times \rho_{impactor}$ (kg/m$^3$) $\times 4\Pi]^{1/3}\}$/1E4 with mass $Os_{impactor}$ derived from (*18*). $[Os]_{impactor}$ is the Os concentration in the impactor (*21*), and $\rho_{impactor}$ is the density of the impactor (*25*).
24. R. Tagle, P. Claeys, *Geochim. Cosmochim. Acta* **69**, 2877 (2005).
25. R. L. Korotev, Washington Univ. (St. Louis); available at http://meteorites.wustl.edu/id/density.htm.
26. In the calculations (*23*), an Os concentration ($[Os]_{impactor}$) of 490 ng/g (*21*) and an average density ($\rho_{impactor}$) of 3.35 g/cm$^3$ (*25*) were representative of an L chondrite meteorite (Popigai LEI event), whereas an Os concentration of 807.5 ng/g (*21*) and an averaged density of 3 g/cm$^3$ (*25*) were used as representative of a carbonaceous chondrite (*28*) for the K-T event.
27. The Ir-based estimate is calculated by knowing the Ir fluence (*3*, *20*), chondritic Ir concentration (Os/Ir = 1.08) (*15*), average density of a chondrite (*25*), and Earth global Ir inventory.
28. F. T. Kyte, *Nature* **396**, 237 (1998).
29. G. S. Collins, K. Wunnemann, *Geology* **33**, 925 (2005).
30. The Ir and Os isotope-based projectile-size estimates probably represent the integrated signal from both the Popigai and the Chesapeake Bay impacts, because spherules believed to derive from both events are found within the single Ir peak at ODP 1090 (*20*). The smaller estimated size for the Chesapeake Bay projectile (*29*) suggests that >90% of the Os and Ir released to the environment was derived from the Popigai event.
31. A. D. Anbar, G. J. Wasserburg, D. A. Papanastassiou, P. S. Andersson, *Science* **273**, 1524 (1996).
32. C.-T. A. Lee, G. J. Wasserburg, F. T. Kyte, *Geochim. Cosmochim. Acta* **67**, 655 (2003).
33. D. S. Ebel, L. Grossman, *Geology* **33**, 293 (2005).
34. In the steady-state, the relation between reservoir size $N$, removal flux $F$, and residence time $t$ is $t = N/F$. This relation implies that the Eocene seawater Os concentration was similar to the modern value, because Eocene estimates of Os burial flux (*35*) and Os residence time made in this work are very similar to recent values (*36*–*38*).
35. T. K. Dalai, G. E. Ravizza, B. Peucker-Ehrenbrink, *Earth Planet. Sci. Lett.* **241**, 477 (2006).
36. T. K. Dalai, G. E. Ravizza, *Geochim. Cosmochim. Acta* **70**, 3928 (2006).
37. S. Levasseur, J.-L. Birck, C. J. Allègre, *Earth Planet. Sci. Lett.* **174**, 7 (1999).
38. R. Oxburgh, *Earth Planet. Sci. Lett.* **159**, 183 (1998).
39. K. A. Farley, A. Montanari, E. M. Shoemaker, C. S. Shoemaker, *Science* **280**, 1250 (1998).
40. For example, the lowest K-T boundary $^{187}Os/^{188}Os$ ever reported (0.137) (*8*) corresponds to a projectile size of greater than 6 km in diameter. On the basis of the unusually large Os concentration at this section, we believe that this section does not accurately reflect the true $^{187}Os/^{188}Os$ concentration of seawater immediately after the K-T event. Instead, we suspect a substantial inventory of particulate impact-derived Os.
41. J. W. Morgan, M. F. Horan, R. J. Walker, J. N. Grossman, *Geochim. Cosmochim. Acta* **59**, 2331 (1995).
42. G. S. Collins, H. J. Melosh, R. A. Marcus, *Meteorit. Planet. Sci.* **40**, 817 (2005).
43. F. T. Kyte, *Deep-Sea Res. II* **49**, 1049 (2002).
44. J. E. T. Channell *et al.*, *Geol. Soc. Am. Bull.* **115**, 607 (2003).
45. H. Pälike *et al.*, *Sci. Res.*, *Proc. Ocean Drill. Prog.* (Ocean Drilling Program, College Station, TX, 2005), vol. 199.
46. We thank the ODP for providing the samples, D. Vonderhaar for technical assistance, E. Scott for his advice and expertise on meteorites, and R. Smith for support. Comments by three anonymous reviewers greatly improved the paper. This work was supported by NSF grants OCE and EAR to G.E.R. and B.P.-E.

**Supporting Online Material**
www.sciencemag.org/cgi/content/full/320/5873/214/DC1
Materials and Methods
SOM Text
Table S1

12 November 2007; accepted 29 February 2008
10.1126/science.1152860

# Linked Reactivity at Mineral-Water Interfaces Through Bulk Crystal Conduction

**Svetlana V. Yanina and Kevin M. Rosso***

The semiconducting properties of a wide range of minerals are often ignored in the study of their interfacial geochemical behavior. We show that surface-specific charge density accumulation reactions combined with bulk charge carrier diffusivity create conditions under which interfacial electron transfer reactions at one surface couple with those at another via current flow through the crystal bulk. Specifically, we observed that a chemically induced surface potential gradient across hematite ($\alpha$-$Fe_2O_3$) crystals is sufficiently high and the bulk electrical resistivity sufficiently low that dissolution of edge surfaces is linked to simultaneous growth of the crystallographically distinct (001) basal plane. The apparent importance of bulk crystal conduction is likely to be generalizable to a host of naturally abundant semiconducting minerals playing varied key roles in soils, sediments, and the atmosphere.

The chemical behavior of mineral-water interfaces is central to aqueous reactivity in natural waters, soil evolution, and atmospheric chemistry and is of direct relevance for maintaining the integrity of waste repositories and remediating environmental pollutants. Traditionally, explorations of fundamental reactions at these interfaces have probed the interaction of water and relevant dissolved ions with crystallographically well-defined mineral surfaces. The pursuit so far has been dominated by the assumption that distinct surfaces of any given crystal behave independently of each other. Except by diffusion through the solution phase or across surface planes, exchange of mass or electron equivalents between sites of differing potential energy at different locations on any given crystal is typically assumed to be negligible. This assumption is nonetheless questionable for the widespread group of minerals that are electrical semiconductors. For example, iron oxides often have moderate to low electrical resistivity (*1*) and have been studied as electrode materials for decades (*2*–*4*). Iron oxide crystal surfaces are chemically reactive with water and ions, leading to solution-dependent charging behavior that differs from one surface type to the next; differing points of zero charge for proton adsorption is but one example (*5*, *6*). This difference should give rise to a surface electric potential gradient ($\Delta\psi_0$) across any crystal that has two or more structurally distinct faces exposed to solution. In principle, this gradient can bias the diffusion of charge carriers (*7*, *8*). Hence, conditions could exist when the gradient across a single crystal is sufficiently large and the electrical resistivity of the material sufficiently

Chemical and Materials Sciences Division, Pacific Northwest National Laboratory, Post Office Box 999, MSIN K8-96, Richland, WA 99352, USA.

*To whom correspondence should be addressed. E-mail: kevin.rosso@pnl.gov